Enhanced kinetics for the LiBH4:MgH2 multi-component hydrogen storage system

Tobias Price, David Grant, Vincent Legrand, Gavin Walker

Enhanced kinetics for the $LiBH_4$:MgH_2 multi-component hydrogen storage system – The effects of stoichiometry and decomposition environment on cycling behaviour

Tobias E.C. Price [a], David M. Grant [a], Vincent Legrand [b], Gavin S. Walker [a,*]

[a] *Energy and Sustainability Research Division, Engineering Faculty, The University of Nottingham, University Park, Nottingham, NG7 2RD, UK*

[b] *Institut Laue Langevin, 6 rue Jules Horowitz, BP 156, 38042 Grenoble cedex 9, France*

In situ neutron diffraction was undertaken on stoichiometric $2LiBD_4 : MgD_2$ and non-stoichiometric $0.3LiBD_4$:MgD_2 with both ratios decomposed under 1 bar deuterium and under dynamic vacuum. The subsequent cycling behaviour under 100 bar D_2 at 400 °C was investigated in situ. Analysis of the uptake through formation of deuterided products showed fast kinetics for the magnesium rich system, 0.3:1, with 90% deuteriding occurring within 10 min. This compares to only 60% deuteriding for the 2:1 sample after 4 h under similar conditions. These results demonstrate the strong influence of stoichiometry in the cycling kinetics compared to decomposition conditions, although the later determines the phase progression.

1. .....

The use of hydrogen as an energy vector offers huge potential for mobile energy generation through fuel cell technology, however this depends on safe, mobile and high density storage of hydrogen. Continued research into hydrogen storage is required to meet US Department of Energy (DOE) targets for mobile hydrogen storage; key goals for storage materials as of 2009 are a gravimetric capacity of 5.5 wt.% and volumetric capacity of 40 g H_2 L^{-1} by 2015 [1]. Research has increasingly turned to high capacity hydrides, particularly low-Z complex hydrides including alanates, amides and borohydrides. Lithium tetrahydridoborate ($LiBH_4$) has strong potential as a useable hydrogen storage material due to its large gravimetric capacity of 18.4 wt%, unfortunately a large energy input is required to release the stored hydrogen (*ca.* $\Delta H = 66.9$ kJ mol^{-1} H_2 [2]) and in practical terms only half the stored hydrogen is released below 600 °C [3]. Many studies have looked at systems based on $LiBH_4$ focusing on catalysts for the dehydrogenation through additions such as oxides, chlorides, fluorides and carbons [4–7].

The high affinity of $LiBH_4$ for reacting with additions makes catalysis difficult as additions tend to form irreversible reaction products. This reactive nature does allow an alternative means of improvement of the system; thermodynamic destabilisation. By offering an alternative reaction with a destabilising addition, lower enthalpy reaction products reduce the enthalpy for decomposition and thus lower the decomposition temperature. This mechanism has been explored by several groups through a variety of additions

* *Corresponding author*. Tel.: +44 115 9513752; fax: +44 1159513800.
E-mail addresses: tobias.price@nottingham.ac.uk (T.E.C. Price), gavin.walker@nottingham.ac.uk (G.S. Walker).

including Au [8], Al [9,10] and MgH_2 [5,11–20]. The use of MgH_2 has an advantage over pure metal additions due to its hydrogen capacity of 7.6 wt% which acts to improve the overall system capacity. Work by Vajo et al. into the system studied a $2LiBH_4$: MgH_2 composition decomposing under a hydrogen atmosphere and found formation of MgB_2 destabilised the system through reaction Eq. (1).

$$2\,LiBH_4 + MgH_2 \leftrightarrows 2\,LiH + MgB_2 + 4\,H_2 \quad (1)$$

Under vacuum conditions however they reported no reaction of the Mg with $LiBH_4$, with the reaction apparently progressing through the straightforward decomposition of the individual component hydrides following reaction 2.

$$2\,LiBH_4 + MgH_2 \rightarrow 2\,LiH + 2\,B + Mg + 4\,H_2 \quad (2)$$

In contrast, work from Nottingham has shown that the magnesium rich 0.3:1 composition decomposes under vacuum through an alternative reaction pathway and liberates all the stored hydrogen via the formation of $Mg_{1-x}Li_x$ alloys [3,18,19] as shown in Eq. (3).

$$0.30LiBH_4 + MgH_2 \leftrightarrows 0.78\,Mg_{0.816}Li_{0.184} + 0.52\,Mg_{0.70}Li_{0.30} + 0.3B + 1.60\,H_2 \quad (3)$$

This reaction provides an alternative destabilisation of $LiBH_4$ because it does not rely on the formation of an intermediate MgB_2 phase but on the formation of $Mg_{1-x}Li_x$ alloys, *viz.* α-alloy $= Mg_{816}Li_{0.184}$ and β-alloy $= Mg_{0.70}Li_{0.30}$. It was thought that only Mg-rich systems would promote the formation of the $Mg_{1-x}Li_x$ alloys, however our results showed formation of these alloys on decomposition of stoichiometric 2:1 ratio decomposed under vacuum [19]. These results also showed formation of MgB_2/LiD on decomposition of 0.3:1 system under deuterium pressure. However, the relative cycling properties were not fully elucidated. This paper reports on a detailed investigation of the cycling behaviour and kinetics for both 2:1 and 0.3:1 ratios on decomposition under D_2 and under a dynamic vacuum in order to understand the effect of stoichiometry and decomposition conditions on the cycling kinetics.

2. Experimental details

Materials used were $LiBH_4$ (Acros Organics, 95%), $^7Li^{11}BD_4$ (Katchem, 98%) and MgH_2 (Alfar Aesar, 98%), which were ball milled and subsequently deuterided (99.8%, D_2, BOC) to form MgD_2 through multiple deuteriding cycles. All handling procedures were conducted under an inert atmosphere. 1.5 g mixtures of $LiBD_4$: MgD_2, with a Li to Mg molar ratio of 0.3:1 and 2:1, were mechanically milled for 1 h under Ar gas at 300 rpm using a Fritsch Rotary P5 ball mill.

Hydrogen release measurements were performed by differential scanning calorimetry (DSC, Netzsch 204 HP Phoenix) and thermogravimetric analysis (TGA, Netzsch 209 F1 Iris) using a heating rate of 10 °C min^{-1}, heating to 585 °C under 1 bar argon flow with a purge rate of 100 cm^3 min^{-1}. Typical sample quantities were 2–5 mg. The samples were run in Al_2O_3 crucibles within hermitically sealed aluminium pans which were loaded in a glove box and the lid was pierced immediately before testing.

Powder neutron diffraction, PND, measurements were performed at the Institut Laue-Langevin (ILL Grenoble, France) using the two-axis D20 instrument in its high flux configuration ($\lambda = 2.42$ Å, flux $= 4.2 \times 10^7$ ns^{-1} cm^{-2}) [21] with scans taken over 5 min periods. Data was analysed using Large Array Manipulation Program (LAMP) version 6, with peak areas analysed using an Excel macro for peak area through temperature ramps and calculation of % conversion during deuteriding. Samples of 1 g mass were loaded into stainless steel 316 L pressure vessels under an inert gas (Ar). The gas manifold system included a MKS 890B Baratron to monitor the pressure in the system. Samples were heated to 550 °C at 1 °C min^{-1} either in a sealed vessel with an initial 1 bar deuterium pressure or decomposed under a dynamic vacuum. Deuteriding was performed at 400 °C under 100 bar D_2 for 4 h. A fresh sample was used for each experiment.

3. Results

The combined DSC and TGA data shown in Fig. 1 shows clear endothermic reactions on heating of the 0.3:1 and 2:1 samples to 550 °C at 10 °C min^{-1} under flowing Ar and the associated weight losses of the samples. Both samples showed two endotherms in the heat flow data appearing at 120–130 °C and 290 °C. The 0.3:1 sample had a large endotherm at 350 °C with a corresponding weight loss of 5.3 wt.%. Two further small endotherms occurred between 400 °C and 550 °C, over which temperature range there was a further weight loss of 3.5 wt.% giving a total of 8.8 wt.%. The 2:1 sample also showed a large endotherm, but at a higher temperature of 375 °C with an associated weight loss of 2.3 wt.%. From 400 to 475 °C there was a broad endothermic event for the 2:1 sample resulting in a weight loss of 6.9 wt.% followed by a more gradual decrease

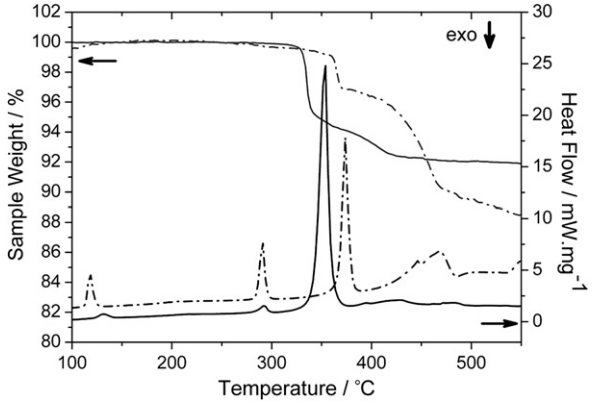

Fig. 1 – DSC and TGA results for 0.3$LiBH_4$: MgH_2 (solid) and 2$LiBH_4$: MgH_2 (dot dashed) run under flowing Ar at 10 °C min^{-1}.

in weight of 1.4 wt.% and a final small endotherm, which gave a total weight loss of 10.6 wt.% overall.

For the *in situ* ND experiments, Fig. 2, sample 0.3:1 run under dynamic vacuum 2(a), the sample followed the decomposition route previously reported for this system [18,19]; *viz.* the hexagonal $LiBD_4$ phase melted forming an amorphous hump in the ND data by 300 °C (visible as a darkened region centred around a d-spacing of 3.2 Å). At 330 °C the MgD_2 phase decomposed resulting in the formation of Mg. Heating to 400 °C the amorphous hump disappeared and LiD appeared. At this point there was a shift to smaller d-spacing in the Mg diffraction lines, signifying the formation of the α-alloy (the Li content increasing until the α-alloy saturation limit was reached, $Mg_{0.814}Li_{0.186}$) and at 550 °C a β-alloy phase appeared ($Mg_{0.70}Li_{0.30}$). The decomposed sample was then cooled to 400 °C and at this temperature 100 bar D_2 was admitted into the sample vessel. This resulted in the formation of a MgD_2 phase and the, corresponding loss of the α-alloy and β-alloy. After 1 h deuteriding the sample was cooled and a $LiBD_{4(hex)}$ pattern was observed on cooling to 250 °C.

For the 2:1 sample run under dynamic vacuum, Fig. 2(b), the progression was similar to that for the 0.3:1 sample. Significant differences were that the α-alloy that formed was completely converted to the β-alloy by 550 °C and that not all the LiD phase decomposed as the phase was still present at 550 °C. On deuteriding, MgD_2 phase did not form until towards the end of the deuteriding period, although on cooling under deuterium the MgD_2 pattern significantly increased in intensity. A weak $LiBD_{4(hex)}$ pattern was also observed on cooling below the melting point of $LiBD_4$, with LiD and Mg patterns being retained.

Decomposing the 2:1 sample under a deuterium pressure Fig. 2(d) followed a similar reaction path to that reported earlier [3,15,18,19]. After the melting of $LiBD_4$ and decomposition of MgD_2, LiD and MgB_2 decomposition products were formed by 520 °C. Deuteriding at 400 °C and 100 bar D_2 resulted in the steady decrease in intensity of the LiD and MgB_2 patterns and a corresponding increase in intensity of the MgD_2 pattern. After 4 h the sample was cooled to 250 °C resulting in formation of a $LiBD_{4(hex)}$ pattern, a weak LiD pattern was also retained on cooling.

For the 0.3:1 sample decomposed under deuterium Fig. 2(c), similar phase changes occurred to those for the 2:1 sample, one notable difference being a residual Mg pattern remaining after formation of MgB_2. On deuteriding at 400 °C the LiD and MgB_2 patterns reduced quickly with a concomitant formation of a $LiBD_4$ amorphous hump and MgD_2 pattern. A $LiBD_{4(hex)}$ pattern was observed on cooling to 250 °C.

Examining the reactions in more detail, Fig. 3 shows the change in phase composition of the samples. For the decompositions under vacuum, Fig. 3(a), the 0.3:1 $LiBD_4$ amorphous hump started to decrease in intensity at *ca.* 390 °C with the concomitant formation of LiD (reaching a maximum at *ca.* 440 °C) and of the α-alloy (initially corresponding to a low Li content reaching the maximum content of 18.4 at.% by 500 °C as determined by the changing d-spacing [22]). As the

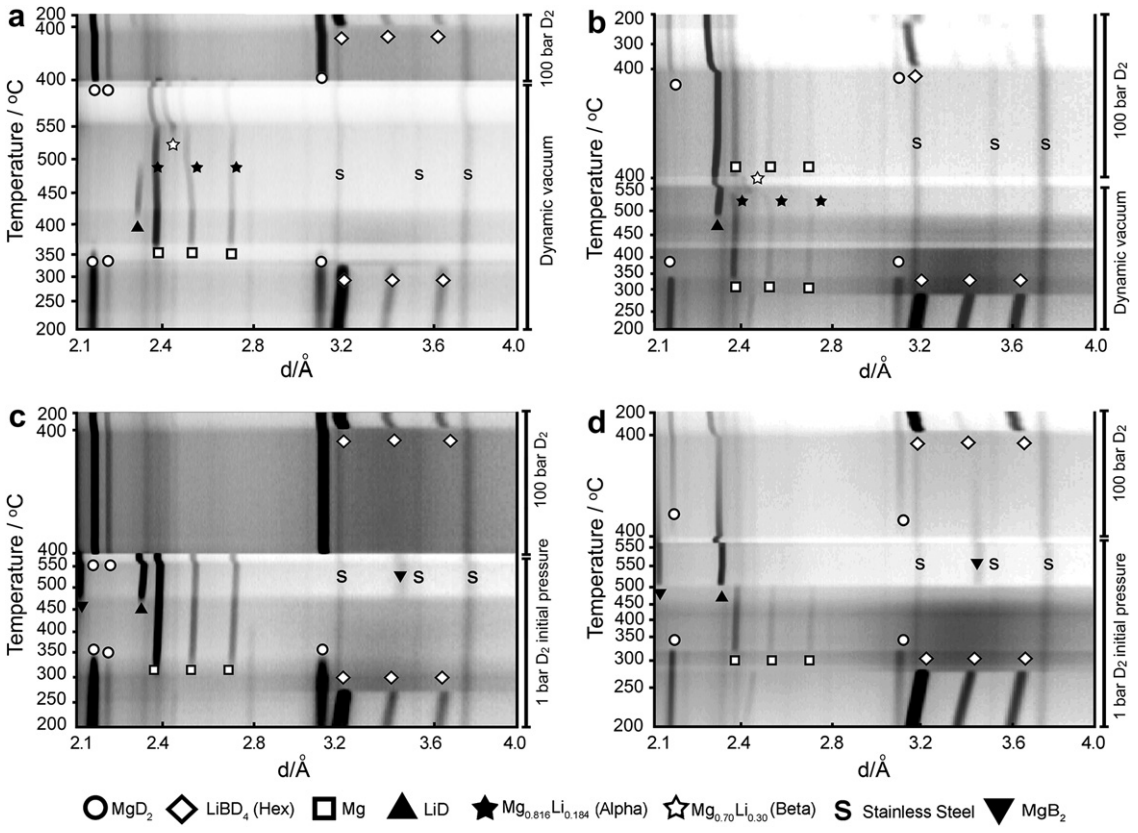

Fig. 2 – Neutron diffraction plots for $LiBD_4$: MgD_2 mixtures a) 0.3:1 decomposed under vacuum, b) 2:1 decomposed under vacuum, c) 0.3:1 decomposed under deuterium and d) 2:1 decomposed under deuterium.

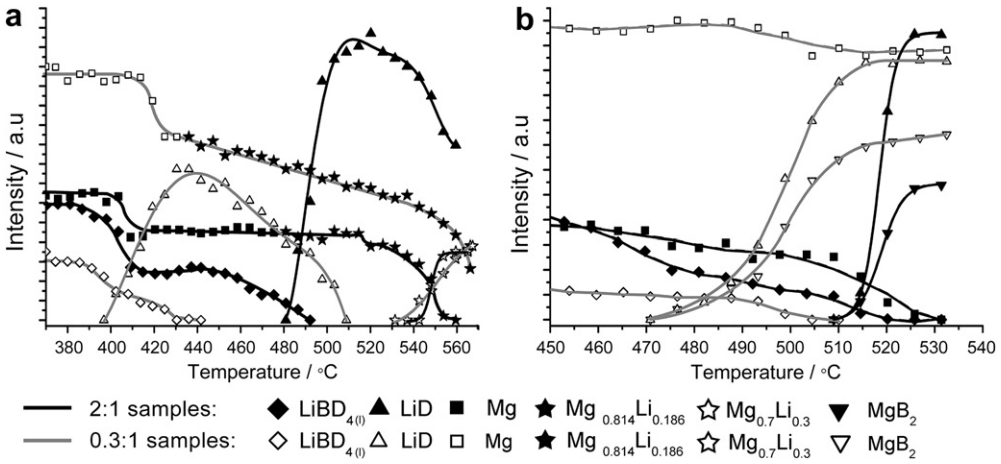

Fig. 3 – Neutron diffraction peak intensity for decomposition of $LiBD_4$: MgD_2 mixtures under (a) dynamic vacuum and (b) deuterium pressure.

magnesium alloys with the lithium the LiD intensity drops off, and at 530 °C the β-alloy started to form, corresponding to a more rapid loss in intensity for the α-alloy. The 2:1 sample followed a similar phase progression but occurring at temperatures of 50 °C higher and most notably with the formation of both the LiD and α-alloy phases only occurring when the $LiBD_4$ amorphous hump had almost disappeared.

For the decompositions under a deuterium pressure, Fig. 3(b), both samples exhibit a decrease in $LiBD_4$ intensity. However, the 0.3:1 sample started forming LiD and MgB_2 decomposition products much earlier, 45 °C lower in temperature than the 2:1 sample. The LiD and MgB_2 for the 0.3:1 sample appeared concomitantly with the loss of the $LiBD_4$ phase, whilst for the 2:1 sample they appeared right at the end of the loss of the $LiBD_4$ phase.

Fig. 4(a) shows the deuteriding behaviour of 0.3:1 samples (decomposed under the two different conditions) charting peak areas during deuteriding at 100 bar D_2 pressure and 400 °C during the first 30 min exposure, and subsequent cooling. For the 0.3:1 sample decomposed under vacuum (top),

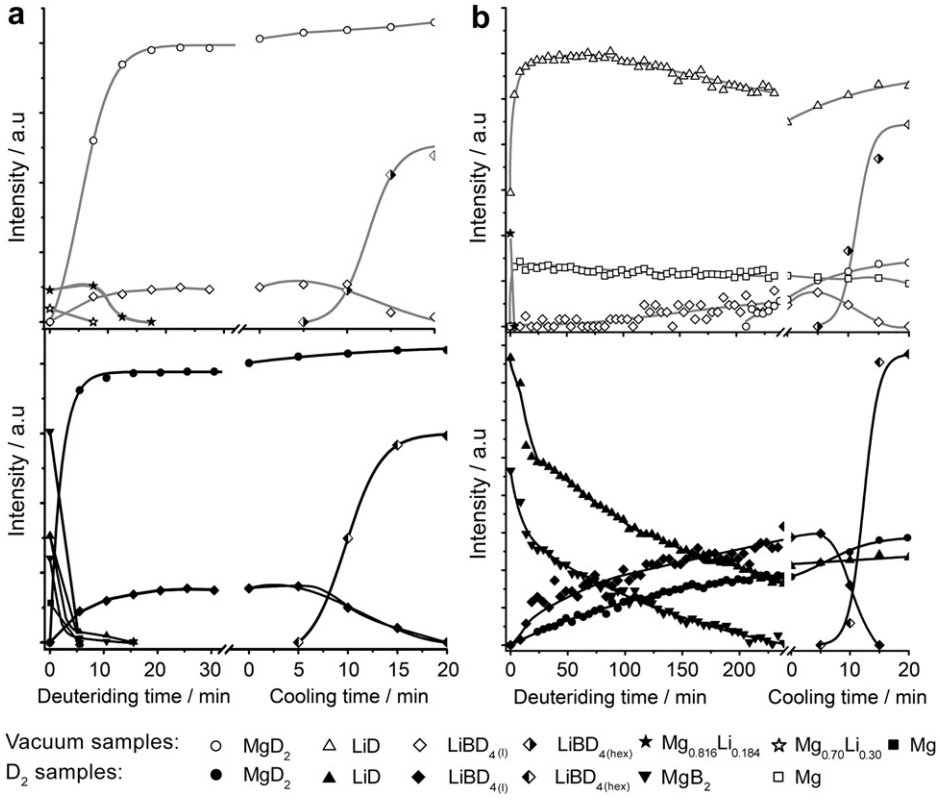

Fig. 4 – Peak intensities during deuteriding at 400 °C and cooling under 100 bar D_2 pressure. (a) 0.3:1 samples decomposed under vacuum (top) and deuterium (bottom), (b) 2:1 samples decomposed under vacuum (top) and deuterium (bottom).

the MgD_2 peak area increased rapidly on addition of the D_2 gas, reaching 90% of its maximum peak area within 15 min, this coincided with the formation of a $LiBD_4$ amorphous hump. The decomposition products α- and β-alloy were lost on formation of $MgD_2/LiBD_4$ with the β-alloy going first, followed by the α-alloy. The 0.3:1 sample decomposed under deuterium pressure (bottom graph in Fig. 4(a)) showed very rapid deuteriding, with the sample losing the $LiD/MgB_2/Mg$ phases and the formation of $MgD_2/LiBD_{4(l)}$ to 90% conversion within 15 min for MgD_2 and 20 min for $LiBD_4$. On cooling, the peak areas increased slightly and $LiBD_{4(hex)}$ peaks appeared.

For the deuteriding of the 2:1 mixture decomposed under deuterium, lower plot of Fig. 4b, there was an initial rapid loss of the LiD phase over the first two scans ($t = 13.5$ min), following this, the rate of reaction greatly slowed and there was only a gradual decrease in LiD intensity, coupled with a corresponding increase in the MgD_2 phase. After 4 h of deuteriding the sample still retained a significant amount of LiD.

The 2:1 sample that had been decomposed under vacuum exhibited an even slower rate of deuteriding. On addition of D_2 gas, the β-alloy was lost within one scan ($t = 3.5$ min) concomitant with the formation of α-alloy phase and a large increase in LiD phase. Subsequently, both Mg and LiD peaks exhibited a very slow drop in intensity over time (17% over 4 h). MgD_2 formed only towards the end of the 4 h deuteriding period and even then it was only a very small proportion of the end product, with the majority of the sample left as unreacted Mg and LiD. The sample was then cooled over 40 min to 250 °C, this caused an increase in the intensities for all peaks. After 5 min cooling $LiBD_{4(hex)}$ peaks formed in both samples.

4. Discussion

The DSC and TGA data in Fig. 1 agrees well with the expected endotherms and weight losses associated with the decomposition of 0.3:1 and 2:1 samples [3,18,19]. The first endotherm at 120–130 °C was due to a phase change of $LiBH_4$ from the low temperature orthorhombic to the high temperature hexagonal phase [23]. The second endotherm appearing at 290 °C was due to the $LiBH_4$ component melting [24]. For the 0.3:1 sample the main endotherm visible on the DSC data at 350 °C was due to the decomposition of the MgH_2 component of the system; which caused a weight loss in the sample of 5.3 wt.% (*cf.* 6.1 wt.% theoretical for the MgH_2 component). The small endotherms following the MgH_2 decomposition were due to $LiBH_4$ decomposition, with an associated weight loss of 3.5 wt.% (*cf.* 3.7 wt.% theoretical for $LiBH_4$ component) giving 8.8 wt.% total. The overall weight loss is lower than the theoretical capacity for the system (9.8 wt.%), the lower MgH_2 weight loss is likely due to a loss of hydrogen through some partial MgH_2 decomposition during the ball milling process. The $LiBH_4$ component weight loss is closer to the theoretical capacity and this small difference can be explained by the purity of the starting materials (*viz.* 95%). The 2:1 sample decomposed in a similar manner, but the MgH_2 peak temperature was 25 °C higher, the lower weight loss of 2.3 wt.% (*cf.* 2.9 wt.% theoretical for MgH_2 component) is again likely due to some partial decomposition during milling. The $LiBH_4$ weight loss of 6.9 wt.% is significantly lower than expected (*cf.* 9.2 wt.% theoretical for $LiBH_4$ component [19]), however, the sample was still losing mass at 585 °C, i.e. the reaction was not complete (supported also by a small endotherm at these temperatures).

The overall reaction determined from the PND data in Fig. 2 for the decomposition under vacuum of the 0.3:1 sample agrees with that reported earlier [3,18,19] as given in Eq. (4).

$$0.30LiBD_4 + MgD_2 \rightarrow 0.78Mg_{0.816}Li_{0.184} + 0.52Mg_{0.70}Li_{0.30} + 0.3B + 1.60D_2 \quad (4)$$

Although the $LiBD_4$ is in the molten state when it decomposed, it was still possible to follow the loss of this phase from the diffraction data by measuring the drop in peak area of the $LiBD_4$ amorphous hump (centred at a d-spacing of 3.4 Å). Fig. 3(a) shows that with the reduction in the amount of the $LiBD_4$ there was a simultaneous formation of LiD. The formation of LiD reaching a maximum peak area at 440 °C, by which time the $LiBD_4$ had fully decomposed to LiD. Then the LiD under vacuum decomposed slowly as Li began alloying with Mg to form $Mg_{1-x}Li_x$ alloys (identified by a decrease in the d-spacing for this phase (see Fig. 2(a)). The LiD peak disappeared at 510 °C. At 530 °C the β-alloy phase began to appear, this marks when the lithium content had increased above the saturation limit for the α-alloy (i.e. 18.4 at.%) and the system moved into a two phase (α + β) region of the phase diagram. Hence there was a coincident loss in the amount of α-alloy present as the higher lithium content β-alloy was formed. Interestingly, the LiD phase was not detected at temperatures above 530 °C, but the formation of the β-alloy phase suggested that there was still some LiD present, but that it was in too small a quantity (<5 mol.%), and/or lacked sufficient long range order to be detected by these relatively short PND scans.

For the decomposition under vacuum of the 2:1 sample, Fig. 2b, the phase progressions from the PND data agree with the overall reaction given by Eq. (5) [19]. Looking in more detail at the phase transitions that occurred, Fig. 3(a), an obvious difference in the sequence of events compared to that for the 0.3:1 sample was that the $LiBD_4$ decomposition did not coincide with the formation of LiD. There was a sharp drop in the PND intensity for the $LiBD_4$ phase just above 400 °C then at 455 °C a more gradual loss in intensity and only towards the end of this did lithium containing decomposition end-products form. This indicates that the $LiBD_4$ was converted into an amorphous intermediate species before the formation of LiD. A shift in the d-spacing for magnesium reflections indicated formation of the α-alloy. This alloying reduced the LiD peak as Li diffused into the Mg and eventually the higher lithium content β-phase, $Mg_{0.70}Li_{0.30}$, formed as the alloy composition moved into the dual phase region, continuing until only the β-alloy remained. It is not clear whether the reaction had stopped at this composition as the LiD peak area was still decreasing but the β-alloy peak area was remaining the same.

$$2\,LiBD_4 + MgD_2 \rightarrow 1.57\,LiD + 1.43\,Mg_{0.70}Li_{0.30} + 2\,B + 4.21D_2 \quad (5)$$

Moving on to the decompositions under an initial deuterium pressure of 1 bar, the *in situ* PND data for the 2:1 sample, Fig. 2c, agrees with the reported overall reaction [5,15,19] as given in Eq. (6).

$$2\,LiBD_4 + MgD_2 \rightarrow 2\,LiD + MgB_2 + 4\,D_2 \quad (6)$$

The 0.3:1 sample run under D_2 progressed through a similar overall reaction, but there was still a Mg phase present at the end of the decomposition because it was in excess of that required to form MgB_2, the reaction therefore progresses through Eq. (7).

$$0.3\,LiBD_4 + MgD_2 \rightarrow 0.3\,LiD + 0.15\,MgB_2 + 0.85\,Mg + 1.45D_2 \quad (7)$$

Fig. 3b shows in more detail the changes in PND intensity for the 2:1 and 0.3:1 decompositions under a deuterium pressure. The two samples each exhibited similar phase changes, but, as with the decomposition under vacuum, the 0.3:1 sample had a concomitant formation of the decomposition products (LiD and MgB_2) with the loss of the $LiBD_4$ phase, but the 2:1 sample only started to form these decomposition products when the intensity for the $LiBD_4$ peak area had almost reached zero. It is interesting to note that the initial loss in intensity of the $LiBD_4$ phase for the 2:1 sample occurred at a similar temperature to the 0.3:1 sample under both decomposition environments. This suggests that the $LiBD_4$ species has become thermally unstable, but for the 0.3:1 sample this results in complete decomposition whereas for the 2:1 sample it results in the formation of an amorphous intermediate phase. Orimo et al. have shown formation of an intermediate when $LiBH_4$ is decomposed on its own. From Raman results and comparing with the calculated phonon density of states they suggested the intermediate was $Li_2B_{12}H_{12}$ [25] forming during the decomposition according to Eq. (8). However this decomposition relies on the formation of LiD which was not evident during the loss of the $LiBD_4$ phase for the 2:1 mixtures suggesting this is unlikely to be the intermediate. Kang et al. have suggested, from DFT results, the potential formation of other intermediate species such as Li_3BH_6 and LiBH as in Eqs. (9) and (10) [26]. Formation of these intermediates does not lead to the formation of LiH, therefore are potential candidates to explain the intermediates formed. However, Li_3BH_6 is unrealistic as B does not like to be 6-coordinate (Kang et al. also found a higher activation energy barrier to the formation of this species), thus LiBH is more likely. However, there is no experimental evidence to show that this species can be formed and it would be a surprising species as this would leave the B in a less favourable electronic configuration.

$$12\,LiBH_4 \rightarrow Li_2B_{12}H_{12} + 10\,LiH + 13\,H_2 \quad (8)$$

$$3\,LiBH_4 \rightarrow Li_3BH_6 + 2\,B + 3\,H_2 \quad (9)$$

$$LiBH_4 \rightarrow LiBH + 3/2H_2 \quad (10)$$

Fig. 4 shows the variation in the phases with time during deuteriding. For the 0.3:1 sample which had been decomposed under vacuum, Fig. 4(a), a strong MgD_2 pattern formed on application of D_2, with a concomitant formation of $LiBD_4$. Both phases reached 90% conversion within 15 min. The loss of the alloy phases (β-alloy first followed by α-alloy) was due to the removal of Li from the alloys. As the Li metal content reduced (due to deuteriding) the β-alloy disappeared transforming to α-alloy, then the α-alloy disappeared as the Li continues to be drawn out of the alloys with the formation of $LiBD_4$. Under these deuteriding conditions any available Mg would be deuterided quickly, hence it would appear that the reaction of the lithium bound in the alloys is controlling the rate at which MgD_2 was formed. It is unclear whether LiD is an intermediate in the formation of $LiBD_4$ as no LiD phase was identified, hence if this phase was involved it reacted quickly and did not form detectable amounts by PND under these experimental conditions. After deuteriding for 1 h (only 30 min shown in Fig. 4(a)), the sample was cooled to 250 °C and a strong $LiBD_{4(hex)}$ pattern appeared as this solid phase crystallised out. Determining the final % conversion was difficult as the peak area of the $LiBD_4$ and MgD_2 patterns was greater than those for the as prepared materials. This discrepancy will be due to a combination of the ball milled as prepared materials being less well ordered and some of the materials decomposing during ball milling (as indicated by the lower weight losses than expected in the TGA results).

Deuteriding also occurred very rapidly for the 0.3:1 sample which had been decomposed under deuterium, in Fig. 4(a) (bottom), forming MgD_2 reaching 90% conversion within 15 min and $LiBD_4$ phases deuteriding slightly slower, reaching 90% within 20 min. Concomitant with $LiBD_4/MgD_2$ formation was loss of the Mg, MgB_2 and LiD phases. Upon cooling to 250 °C a $LiBD_{4(hex)}$ phase crystallised out.

Fig. 4(b) shows the progression of deuteriding for the 2:1 sample decomposed under vacuum and under a D_2 pressure. It is immediately obvious that the rate of deuteriding was over an order of magnitude slower than for the 0.3:1 sample. For the 2:1 sample decomposed under vacuum, a sharp increase in the LiD peak area was detected as the β-alloy reverted to a magnesium phase (as corroborated by the d-spacing for the (002) reflection). This indicated that the lithium in the alloy was preferentially deuterided (reflecting the higher reactivity of Li) forming LiD and Mg. However, after this initial reaction there was only a very slow drop in LiD/Mg intensity consistent with the slow formation of $LiBD_4$. It is only towards the end of deuteriding that MgD_2 peaks can be seen. It is surprising that the Mg does not deuteride more quickly and these slow kinetics must be due to the diffusion of lithium out of the β-alloy forming a passivating layer of lithium deuteride around the magnesium, hindering the formation of MgD_2. On cooling, contraction of the passivating LiD layer would lead to cracking in this layer due to the comparatively large difference in the coefficient of thermal expansion between the two phases ($Mg = 25 \times 10^{-6}\,K^{-1}$, $LiD = 46 \times 10^{-6}\,K^{-1}$ [27]). These cracks would expose the Mg core enabling deuteriding of the metal forming more MgD_2. This process would also be accelerated by the subsequent expansion of the magnesium containing core (upon deuteriding) leading to further cracking and potentially delamination of the LiD layer (formation of magnesium hydride results in a 33% volume expansion [28]). On cooling to 250 °C a small $LiBD_{4(hex)}$ phase appeared, showing partial reversibility (approximately 10% $LiBD_4$ and 30% MgD_2 completion of reaction as calculated from peak area analysis of the main peaks at 150 °C before and after cycling). The poor reversibility of the 2:1 multi-component system when decomposed under vacuum agrees with reports from other groups under similar conditions [5].

For the 2:1 sample decomposed under deuterium, Fig. 4(d), the decomposition products of LiD and MgB_2 were deuterided, there was initially a rapid loss of both phases over the first 11 min, followed by a slower steady drop in intensity for the remainder of the deuteriding time (4 h in total). The loss of these two phases was concomitant with the formation of MgD_2 and $LiBD_4$. The fast kinetics is likely to be associated with the initial reaction of deuterium at the surface of the sample, but the rate of the subsequent reaction is decreased because the high $LiBD_4$ content material may result in the encapsulation of MgB_2 within a LiD matrix, hindering the mass transport required for further reaction. It is interesting that no slowing of kinetics was observed for the 0.3:1 ratio, probably due to the lower $LiBD_4$ content leading to an insufficient amount of LiD being produced to form a coherent LiD matrix. On cooling the 2:1 sample after deuteriding, $LiBD_{4(hex)}$ was formed, but there was still some LiD present, with approximately 50% $LiBD_4$ and 43% MgD_2 re-formed after cycling.

5. Conclusions

These results have shown that the stoichiometry of the $LiBD_4$: MgD_2 mixtures has a great effect on the reaction pathway and the kinetics for cycling. The $LiBD_4$ for the 0.3:1 mixtures decomposes directly to LiD (and MgB_2 when under D_2). In contrast the 2:1 samples did not show the same direct decomposition route, indicating the formation of an intermediate species [25,26] which slowed down the decomposition reaction. For the reverse reaction, the 0.3:1 samples deuterided very quickly under the conditions investigated with 90% conversion within 15 min. The 2:1 samples showed incomplete deuteriding reactions with conversions of only 50% after 4 h for the sample containing MgB_2 and for the decomposition under vacuum, only 10% of the initial $LiBD_4$ was formed. Mass transport is an important issue with these low conversions and the formation of diffusion barrier layers from the deuteriding products is a major contributing factor.

Acknowledgments

Funding and support from EPSRC Supergen UKSHEC. We would also like to thank Dr. Thomas Hanson for his support on the D20 neutron diffractometer at Institut Laue-Langevin., ILL expt number 5-25-171.

REFERENCES

[1] Dilich S. 2009. Hydrogen program and vehicle technologies program annual merit review and peer evaluation meeting. Annual Merit Review and Peer Evaluation Meeting, Arlington, Virginia, USA.
[2] Chase MW. NIST-JANAF thermochemical tables. 4th ed. New York: American Institute of Physics; 1998.
[3] Yu XB, Grant DM, Walker GS. A new dehydrogenation mechanism for reversible multicomponent borohydride systems: the role of Li–Mg alloys. Chem Commun; 2006:3906–8.
[4] Au M, Jurgensen A. Modified lithium borohydrides for reversible hydrogen storage. J Phys Chem B 2006;110:7062–7.
[5] Vajo JJ, Skeith SL, Mertens F. Reversible storage of hydrogen in destabilized $LiBH_4$. J Phys Chem B 2005;109:3719–22.
[6] Fang ZZ, Kang XD, Dai HB, Zhang MJ, Wang P, Cheng HM. Reversible dehydrogenation of $LiBH_4$ catalyzed by as-prepared single-walled carbon nanotubes. Scr Mater 2008;58: 922–5.
[7] Yin L, Wang P, Fang Z, Cheng H. Thermodynamically tuning $LiBH_4$ by fluorine anion doping for hydrogen storage: a density functional study. Chem Phys Lett 2008;450: 318–21.
[8] Mosegaard L, Moller B, Jorgensen JE, Filinchuk Y, Cerenius Y, Hanson JC, et al. Reactivity of $LiBH_4$: in situ synchrotron radiation powder X-ray diffraction study. J Phys Chem C 2008;112:1299–303.
[9] Kim JW, Friedrichs O, Ahn J-P, Kim DH, Kim SC, Remhof A, et al. Microstructural change of $2LiBH_4$/Al with hydrogen sorption cycling: separation of Al and B. Scr Mater 2009;60: 1089–92.
[10] Kang X-D, Wang P, Ma L-P, Cheng H-M. Reversible hydrogen storage in LiBH4 destabilized by milling with Al. Appl Phys A: Mater Sci Process 2007;89:963–6.
[11] Fan M-Q, Sun L-X, Zhang Y, Xu F, Zhang J, Chu H-l. The catalytic effect of additive Nb_2O_5 on the reversible hydrogen storage performances of $LiBH_4$–MgH_2 composite. Int J Hydrogen Energy 2008;33:74–80.
[12] Wang P-J, Fang Z-Z, Ma L-P, Kang X-D, Wang P. Effect of SWNTs on the reversible hydrogen storage properties of $LiBH_4$–MgH_2 composite. Int J Hydrogen Energy 2008;33:5611–6.
[13] Wang P-J, Fang Z-Z, Ma L-P, Kang X-D, Wang P. Effect of carbon addition on hydrogen storage behaviors of Li–Mg–B–H system, in press. doi:10.1016/j.ijhydene.2009.1007.1041.
[14] Barkhordarian G, Klassen T, Dornheim M, Bormann R. Unexpected kinetic effect of MgB_2 in reactive hydride composites containing complex borohydrides. J Alloys Compd 2007;440:18–21.
[15] Bosenberg U, Doppiu S, Mosegaard L, Barkhordarian G, Eigen N, Borgschulte A, et al. Hydrogen sorption properties of MgH_2–$LiBH_4$ composites. Acta Mater 2007;55:3951–8.
[16] Pinkerton FE, Meyer MS, Meisner GP, Balogh MP, Vajo JJ. Phase boundaries and reversibility of $LiBH_4$/MgH_2 hydrogen storage material. J Phys Chem C 2007;111:12881–5.
[17] Yu XB, Grant DM, Walker GS. Low-temperature dehydrogenation of $LiBH_4$ through destabilization with TiO_2. J Phys Chem C 2008;112:11059–62.
[18] Price TEC, Grant DM, Telepeni I, Yu XB, Walker GS. The decomposition pathways for $LiBD_4$–MgD_2 multicomponent systems investigated by in situ neutron diffraction. J Alloys Compd 2009;472:559–64.
[19] Walker GS, Grant DM, Price TEC, Legrand V, Yu X. High capacity multicomponent hydrogen storage materials investigation of the effect of stoichiometry and decomposition conditions on the cycling behaviour of $LiBH_4$–MgH_2. J Power Sources 2009;189:902–8.
[20] Yu XB, Wu Z, Chen QR, Li ZL, Weng BC, Huang TS. Improved hydrogen storage properties of $LiBH_4$ destabilized by carbon. Appl Phys Lett 2007;90. 034106.
[21] Hansen TC, Henry PF, Fischer HE, Torregrossa J, Convert P. The D20 instrument at the ILL: a versatile high-intensity two-axis neutron diffractometer. Meas Sci Technol; 2008:034001.
[22] Herbstein FH, Averbach BL. The structure of lithium–magnesium solid solutions–I: measurements on the Bragg reflections. Acta Metall 1956;4:407–13.
[23] Hartman MR, Rush JJ, Udovic TJ, Bowman JRC, Hwang S-J. Structure and vibrational dynamics of isotopically labeled lithium borohydride using neutron diffraction and spectroscopy. J Solid State Chem 2007;180:1298–305.

[24] Schlesinger HI, Brown HC. Metallo borohydrides. III. Lithium borohydride. J Am Chem Soc 1940;62:3429–35.
[25] Orimo S-I, Nakamori Y, Ohba N, Miwa K, Aoki M, Towata S-i, et al. Experimental studies on intermediate compound of $LiBH_4$. Appl Phys Lett 2006;89:021920–3.
[26] Kang JK, Kim SY, Han YS, Muller RP, Goddard III WA. A candidate $LiBH_4$ for hydrogen storage: crystal structures and reaction mechanisms of intermediate phases. Appl Phys Lett 2005;87. 111904.
[27] Lide D. CRC handbook of chemistry and physics. 88th ed. CRC; 2007.
[28] Zlotea C, Lu J, Andersson Y. Formation of one-dimensional MgH_2 nano-structures by hydrogen induced disproportionation. J Alloys Compd 2006;426:357–62.